Int. J. Heat Mass Transfer. Vol. 30, No. 8, pp. 1655–1662, 1987
Printed in Great Britain

0017–9310/87 $3.00 + 0.00

Mixed convection between horizontal plates—II. Fully developed flow

KUAN-CHENG CHIU,† JALIL OUAZZANI† and FRANZ ROSENBERGER†
Department of Physics, University of Utah, Salt Lake City, UT 84112, U.S.A.

(*Received* 16 *June* 1986 *and in final form* 28 *January* 1987)

Abstract—Fully developed velocity profiles of longitudinal convection rolls in mixed convection between horizontal plates were measured in nitrogen by laser Doppler anemometry for a range $2472 < Ra < 8300$ and $15 < Re < 150$. It is shown analytically and experimentally that the transverse velocities of the longitudinal convection rolls are independent of the forced flow. The experimentally and numerically obtained w-profiles ($Pr = 0.71$) are in good agreement with theoretical predictions ($Pr \to \infty$) and other experimental results ($Pr = 11.1$ and 930) for Rayleigh–Benard convection. A detailed study of the longitudinal velocity modulation $\Delta u[w_{max}(Ra), Re]$ is presented. Also, asymmetric roll patterns were found in spite of the small temperature differences used between the horizontal plates.

1. INTRODUCTION

FULLY developed three-dimensional mixed convection between horizontal parallel plates, isothermally heated from below and cooled from above, plays a significant role in various technological processes, such as the chemical vapor deposition of solid layers [1, 2], or the cooling of electronic equipment [3]. In the preceding paper [4] we have investigated entrance effects in such flows. Here we are concerned with the fully developed region.

Before addressing mixed convection, we will review some closely related results obtained for purely buoyancy-induced flow between horizontal plates, i.e. Rayleigh–Benard (R–B) flow, that are important for this work. A general discussion of R–B convection can be found in the monograph by Chandrasekhar [5] and recent reviews by Normand *et al.* [6], and Berge and Dubois [7]. The velocity field of R–B convection rolls has been studied over the last 20 years. Theoretical calculations of the velocity amplitudes were performed by Busse [8], Normand *et al.* [6], and Degiorgio [9]. Busse's calculation [8] is based on an infinite Prandtl number ($Pr \to \infty$). Thus, the momentum advection is neglected. Normand *et al.* [6] also assumed an infinite Pr and limited the Rayleigh number, Ra, to just slightly above Ra_c (critical Ra for R–B convection). They used the usual expansion in terms of a small parameter $\varepsilon = (Ra - Ra_c)/Ra_c$ (reduced Rayleigh number) for the first three harmonics and gave the amplitude of each velocity mode. Degiorgio's treatment [9] is also limited to the region not too far above Ra_c where a single (first harmonic) convection mode prevails. Following the single mode assumption, Degiorgio took the governing equations for the critical state (which is Pr independent) and solved for the amplitude of the vertical velocity. Experimental determinations of R–B velocities were first performed by Dubois and co-workers [10, 11]. They used laser Doppler anemometry (LDA) to measure the velocity distribution in silicone oil near 25°C ($Pr = 930$) and water near 4°C ($Pr = 11.1$).

When an externally forced laminar flow is superimposed on the buoyancy-driven flow between the plates, for $Ra_{c,t}(Re) > Ra$ (where $Ra_{c,t}$ represents the critical Ra for the transverse convection rolls and is a function of Re, Reynolds number, as shown in our previous paper [4]) only the longitudinal convection rolls (with axes parallel to the forced flow direction) are present. Mori and Uchida [12] have analytically studied this mixed (longitudinal) convection problem by means of a quasi-linear approximation and determined the velocity amplitude by Stuart's energy integral method. Their analysis yields a $1/Re$ dependence of the transverse velocities v and w, and an Re independence of the modulation amplitude of u, Δu. (See Fig. 1 for the coordinate system and definition of velocity components.) However, Braaten and Patankar [3] have pointed out that: "... the (v and w) solution is not affected by the Reynolds number of the axial flow. This is a characteristic of all fully developed duct flows". We must add that this statement is restricted to (horizontal) longitudinal convection rolls.

Since fully developed longitudinal mixed convection is essentially a 2-D flow, Ogura and Yagihashi [13], Hwang and Cheng [14], and Fukui *et al.* [15] conducted 2-D numerical studies of this problem. Their results for the flow pattern and temperature field, based on the Boussinesq approximation, agree well with experimental data [12, 15, 16]. But all these numerical and experimental results are only concerned with the flow pattern and temperature profile for specific Ra and Re numbers. No relations $\Delta u(Ra, Re)$ have been given so far.

† Now at Center for Microgravity and Materials Research, University of Alabama in Huntsville, Huntsville, AL 35899, U.S.A.

NOMENCLATURE

g	gravitational acceleration, 980 cm s^{-2}
H	height of the channel, 1.58 cm
L_2	entrance length for fully developed flow, equation (6)
P_0	mean pressure
Pr	Prandtl number, ν/κ
Ra	Rayleigh number, $\beta g \Delta T H^3/\nu\kappa$
Ra_c	critical Ra for R–B convection, 1708
$Ra_{c,t}$	critical Ra for transverse convection rolls
Re	Reynolds number, $u_0 H/\nu$
T_0	average temperature, $(T_h+T_c)/2$
T_c	temperature of the cold plate and isothermal section
T_h	temperature of the hot plate
ΔT	$T_h - T_c$
u, v, w	velocity component in x-, y-, z-direction
u_0	average velocity, $u_{max}/1.5$, to simulate the laterally unbound configuration
u_{max}	maximum u-velocity at $x = -3H$
Δu	modulation amplitude of u-velocity at $z = H/2$ in fully developed mixed flow region
W	width of the channel, 15.24 cm
w_n	expansion coefficient of the nth mode, equation (9)
w_{max}	$(w_{max(a)}+w_{max(d)})/2$
$w_{max(a)}$	absolute value of maximum w-velocity for the ascending flow
$w_{max(d)}$	absolute value of maximum w-velocity for the descending flow
x, y, z	Cartesian coordinates.

Greek symbols

β	thermal expansion coefficient [K^{-1}]
ε	reduced Rayleigh number, $(Ra-Ra_c)/Ra_c$
κ	thermal diffusivity [cm^2 s^{-1}]
ν	kinematic viscosity [cm^2 s^{-1}]
ρ	density of gas [g cm^{-3}]
σ	dimensionless time constant, equation (10).

Abbreviations

2-D	two-dimensional
AR	aspect ratio = width/height
LDA	laser Doppler anemometry
R–B	Rayleigh–Benard.

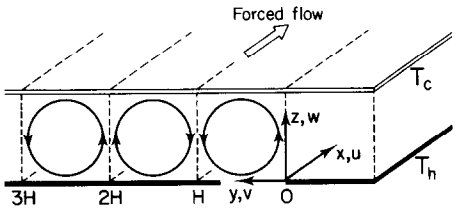

FIG. 1. Flow configuration and coordinate system.

This paper serves several purposes. First, we give an explicit mathematical analysis of the problem. Then, we present experimentally determined velocity profiles for nitrogen ($Pr = 0.71$) in the range $2472 < Ra < 8300$ and $15 < Re < 150$. Furthermore, we deduce a relation $\Delta u[w_{max}(Ra), Re]$, where w_{max} is an average of the absolute values of maximum w-velocity in the ascending and descending flows. Also, 2-D numerical results ($Pr = 0.71$) for v- and w-profiles are obtained and compared with our experimental data. Then, our results are compared with those of other experimental works for $Pr = 11.1$ and 930 [10, 11], and with theoretical predictions for the 2-D R–B flow based on either an infinite Pr [6, 8] or a single mode assumption [9]. Finally, we present asymmetric roll patterns observed in spite of the small temperature difference used between the horizontal plates.

2. MATHEMATICAL ANALYSIS

We base our analysis on the Boussinesq approximation. The physical properties are assumed to be constant. According to the definition of a fully developed flow, the first and second derivatives of u, v, w, T with respect to x are zero. This assumption limits the solutions to longitudinal convection rolls. The drive for the forced flow, $\partial P/\partial x$, is assumed to be constant throughout. With these simplifications, the governing equations for the steady, fully developed, longitudinal convection rolls become

$$\frac{\partial v}{\partial y} + \frac{\partial w}{\partial z} = 0 \tag{1}$$

$$v\frac{\partial u}{\partial y} + w\frac{\partial u}{\partial z} = -\frac{1}{\rho}\frac{\partial P}{\partial x} + \nu\left(\frac{\partial^2 u}{\partial y^2} + \frac{\partial^2 u}{\partial z^2}\right) \tag{2}$$

$$v\frac{\partial v}{\partial y} + w\frac{\partial v}{\partial z} = -\frac{1}{\rho}\frac{\partial P}{\partial y} + \nu\left(\frac{\partial^2 v}{\partial y^2} + \frac{\partial^2 v}{\partial z^2}\right) \tag{3}$$

$$v\frac{\partial w}{\partial y} + w\frac{\partial w}{\partial z} = -\frac{1}{\rho}\frac{\partial P}{\partial z} + \nu\left(\frac{\partial^2 w}{\partial y^2} + \frac{\partial^2 w}{\partial z^2}\right) - g[1-\beta(T-T_c)] \tag{4}$$

$$v\frac{\partial T}{\partial y} + w\frac{\partial T}{\partial z} = \kappa\left(\frac{\partial^2 T}{\partial y^2} + \frac{\partial^2 T}{\partial z^2}\right). \tag{5}$$

Note that only equation (2) contains the longitudinal velocity u. Hence, equations (1) and (3)–(5) are uncoupled from equation (2), i.e. they can be solved independently of equation (2). Actually these four equations are identical to the governing equations for the steady, 2-D R–B convection rolls with their axes

parallel to the x-direction. Thus, the critical Ra for the longitudinal convection rolls is independent of Re and is equal to Ra_c [14, 17]; and the solutions of the transverse velocities of the steady, fully developed, longitudinal convection rolls are identical to those of the steady 2-D R–B convection. The u-profile can be obtained from equation (2) by substituting the other four functions into it. Equation (2) shows, in turn, how the u-velocity is modulated by the transverse velocities.

On inclusion in the analysis of temperature-dependent properties, the independence of the transverse components v and w is retained. The system of equations (1)–(5) is then expanded by three temperature–property relations for ρ, ν and κ, without changes in the symmetry of the interaction terms.

For a numerical analysis of the steady-state, 2-D R–B convection, we employed the finite element code FIDAP [18]. A Boussinesq approximation was used with the physical properties evaluated at the average temperature. No-slip ($v = w = 0$) and constant temperature conditions ($T = T_h$, $T = T_c$, respectively) were invoked on the boundaries $z = 0, H$. To simulate a laterally unbound configuration, symmetric boundary conditions ($\partial w/\partial y = \partial T/\partial y = 0$, and $v = 0$) were used at $y = 0, H$. A 21×21 mesh was employed in this calculation domain. To ascertain non-zero solutions, initial perturbations of the simple form, $w = A$ at $y = 0$ and $w = -A$ at $y = H$, where $2 < A/w_{max} < 4$, were found useful.

3. EXPERIMENTAL APPARATUS AND TECHNIQUE

The details of the experimental arrangement and LDA set-up have been described in ref. [4]. For the comparison with laterally unbound configuration, we focus on the flow in the central region only. Because of the high aspect ratio (AR = width/height = 10) of the channel and the opaqueness of the top and bottom plates, a small viewing angle between the laser beams has to be used to measure the vertical w-velocity into the middle of the channel. Hence, we used a beam spacing of 22 mm and a focal length of 250 mm for the transmitting lens. This, however, results in a measuring-volume length of 4.8 mm. With off-axis collection this was effectively reduced to 0.4 mm. For details see ref. [19].

4. RESULTS AND DISCUSSION

As we have shown in ref. [4], the entrance length for the steady, fully developed flow can be given as

$$L_2 = (0.68 \pm 0.07) H \varepsilon^{-0.69 \pm 0.02} Re^{0.96 \pm 0.03} \quad (\varepsilon > 0). \quad (6)$$

Hence, all data presented in this paper are measured at axial positions of $x > L_2$.

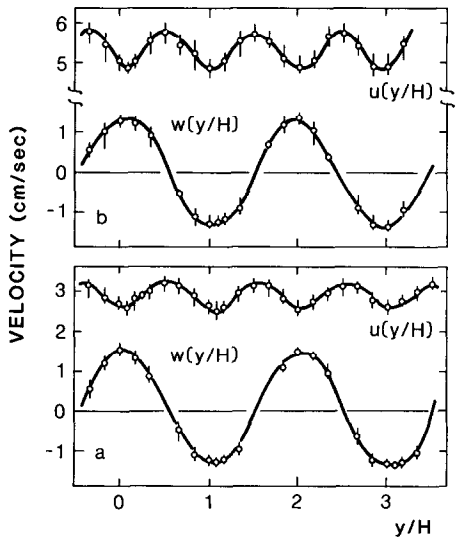

FIG. 2. Velocity profiles of $u(y)$ and $w(y)$ measured at $z = H/2$ and $Ra = 2472$ for: (a) $Re = 18.1$; (b) $Re = 32.5$.

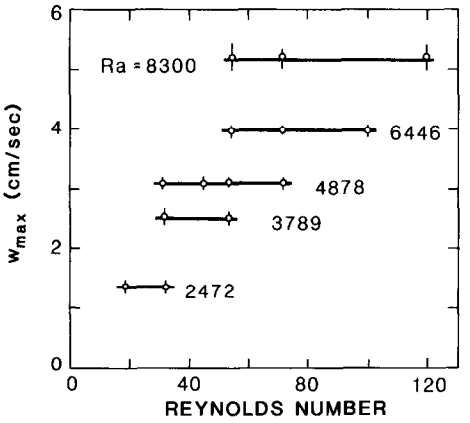

FIG. 3. Re independence of w_{max}.

4.1. *Re independence of transverse velocity*

In order to investigate whether the transverse velocity is independent of Re, the velocity profiles, $u(y)$ and $w(y)$, were measured at $z = H/2$ for different Res at fixed Ras. Figure 2 shows a comparison of the profiles for two different Res at $Ra = 2472$. One sees that, in contrast to u, w is independent of Re. Note also that the w-velocity profile is a sinusoidal function of y with a wavelength equal to $2H$, which is characteristic of the first mode of the R–B convection rolls. Figure 3 further emphasizes the Re independence of w by representations of w_{max} data for a wider range in Re and various values of Ra, $2472 < Ra < 8300$. Note that in pure R–B convection in gases the flow is unsteady for $Ra > 4800$ [20]. In our mixed convection experiments, for $Ra_{c,t}(Re) > Ra$ [4], the longitudinal rolls are steady even at $Ra = 8300$. Hence, as suggested earlier [12], the superposition of a forced flow stabilizes the R–B convection.

4.2. *Modulation of longitudinal velocity*

Experimental data for the modulated $u(y, z)$ velocity profile across a pair of rolls are depicted in Fig.

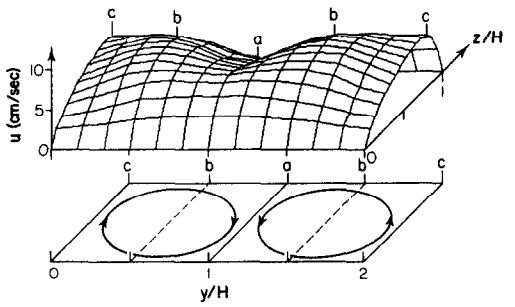

FIG. 4. u-Velocity measured across a pair of rolls (see lower part) for $Re = 44.8$ and $Ra = 4878$: (a)–(c) denotes planes for velocity profiles in Fig. 5.

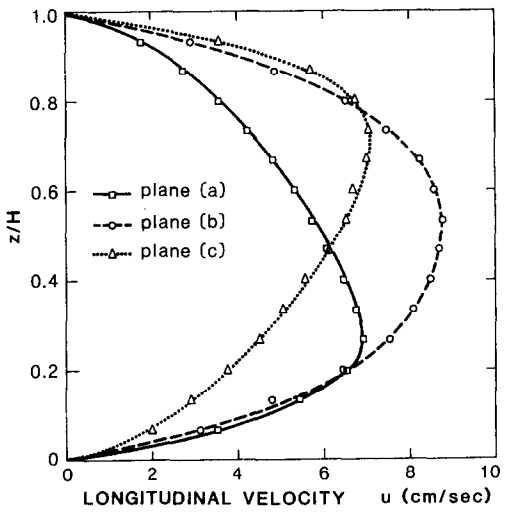

FIG 5. Vertical sections (x–z planes spaced by $H/2$) through the u-surface of Fig. 4.

4. Vertical sections (spaced by $0.5H$) through this u-surface are given in Fig. 5, curves (a)–(c). From these (Figs. 4 and 5) one sees that the peaks in $u(z)$ for the ascending (descending) flow are shifted up (down) with respect to $z = 0.5H$. This is due to the momentum coupling between the forced and R–B convection governed by equation (2). This finding agrees with other numerical and experimental results [12, 15]. It is also interesting that the wavelength of u at $z = 0.5H$, as shown in Fig. 2, equals H, whereas w shows a $2H$ periodicity. This is because only at $z = 0.5H$ the ascending flow and descending flow of the R–B convection give the same contribution to the modulation in the u-velocity profile (Fig. 4). This symmetry follows, of course, also from the Boussinesq approximation. Therefore, the u-velocity profile at $z = 0.5H$ can be expressed as

$$u(y) = u_0 + \Delta u \cos(2\pi y/H).$$

Furthermore, the modulation amplitude, Δu, resulting from the interplay of forced (Re) and R–B convection ($w_{\max}(Ra)$, see next section), can be written as $\Delta u = C[w_{\max}(Ra)]^n Re^m$. From the experimental data (see Table 1) we have determined the constant C and

Table 1. Modulation amplitude at $z = 0.5H$ in the fully developed region

Ra	$w_{\max}$ (cm s^{-1})	Re	Δu (cm s^{-1})	
2472	1.35	18.1	0.24 ± 0.01†	0.29 ± 0.02‡
		32.5	0.41 ± 0.02	0.45 ± 0.04
3789	2.50	17.7	0.48 ± 0.02	
		31.8	0.71 ± 0.04	
		53.8	1.06 ± 0.05	1.36 ± 0.12
4878	3.08	31.6	0.82 ± 0.10	0.94 ± 0.06
		44.8	1.48 ± 0.08	1.40 ± 0.04
		52.8	1.60 ± 0.08	1.68 ± 0.08
		71.7	1.88 ± 0.08	
6446	3.98	53.4		1.88 ± 0.16
		71.3		2.56 ± 0.12
8300	5.14	53.4	2.54 ± 0.16	2.37 ± 0.12
		71.7	3.20 ± 0.16	2.96 ± 0.16
		120.2	4.92 ± 0.33	4.90 ± 0.28

† For measurement with beam spacing = 50 mm.
‡ For measurement with beam spacing = 22 mm.

the exponents n and m by a least-square method and obtained

$$\Delta u = (0.016 \pm 0.001)[w_{\max}(Ra)]^{1.00 \pm 0.03} Re^{0.86 \pm 0.03}. \quad (7)$$

4.3. *Comparison of $w_{\max}$ with* R–B *velocities*

We have obtained numerical solutions for a single R–B convection roll for seven different Ras covering the range $1800 < Ra < 8297$. The results for $Ra = 8297$ are depicted in Figs. 6(a)–(c). As expected, an anti-symmetric flow pattern with respect to the center of the roll is obtained. We also see a reversed temperature gradient in the central region of the roll (Fig. 6(c)) due to the heat advection of the longitudinal roll. This was analytically predicted by Mori and Uchida [12] and experimentally confirmed by Ostrach and Kamotani [16] as well as Fukui *et al.* [15]. Our results further reveal that this reversal in the temperature gradient occurs at $Ra > 3800$. The $w(y)$ profile at $z = 0.5H$ is shown in Fig. 6(b). We express this profile in terms of a Fourier series as

$$w(y, z = 0.5H) = \sum_{n=1,3,5} a_n \cos\left(\frac{n\pi y}{H}\right). \quad (8)$$

The vanishing of the even terms reflects the anti-symmetry of $w(y)$. Closer inspection of the numerical solutions, however, reveals that for $Ra > 4878$ the absolute extrema for w lie one grid plane, i.e. $\Delta z = 0.05H$, above (ascending flow) and below (descending flow) midheight $z = 0.5H$. These $w_{\max}$ values exceed the w velocities at $z = 0.5H$ only by 0.6% even for the largest $Ra = 8297$. Hence, we ignore these small deviations and use equation (8) also for $w_{\max}$. Based on Landau's mean-field theory [6, 7], the coefficients a_n in equation (8) are proportional to $(\kappa/H)\varepsilon^{n/2}$. With these we obtain from equation (8)

$$w_{\max} = w_1 \frac{\kappa}{H}\varepsilon^{1/2} + w_3 \frac{\kappa}{H}\varepsilon^{3/2} + w_5 \frac{\kappa}{H}\varepsilon^{5/2} + \ldots. \quad (9)$$

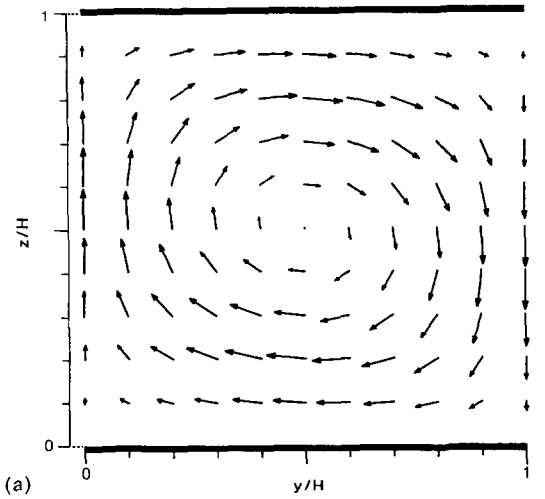

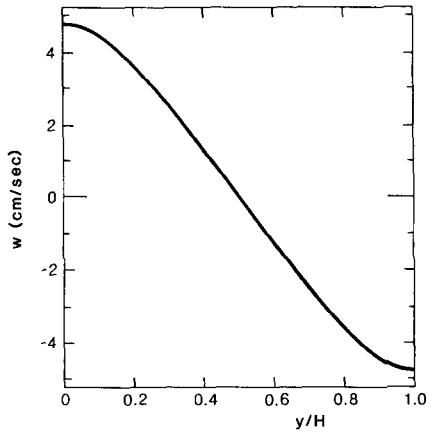

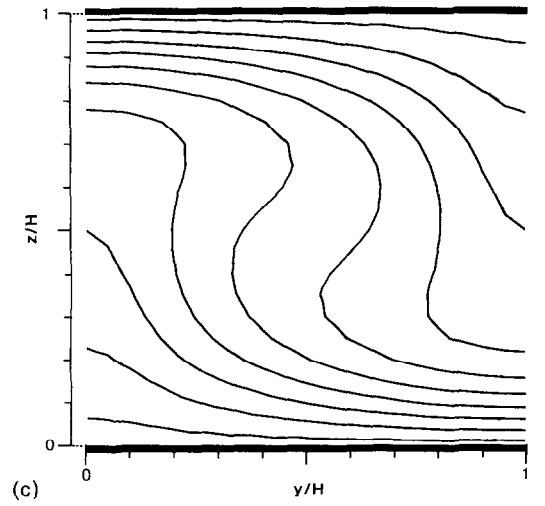

FIG. 6. Numerical results for one of the rolls at $Ra = 8297$: (a) velocity field (v, w) in y–z plane, only 1/4 of the grid points are shown, $w_{max} = 4.82$ cm s^{-1}; (b) $w(y/H)$ profile at $z = H/2$; (c) isotherm profiles in the y–z plane, the temperature difference between two isotherms is $0.1\Delta T$, except between the upper (and the lower) wall and the closest isotherms where the difference is $0.05\Delta T$.

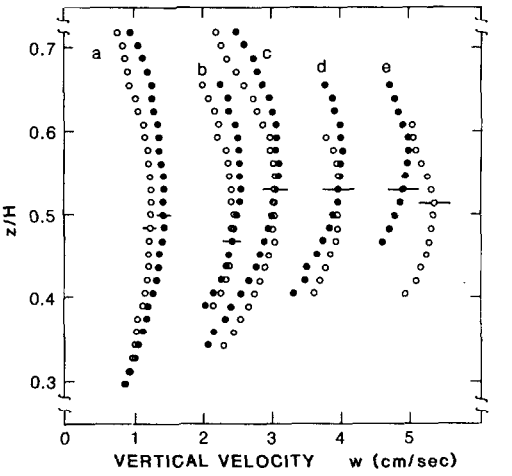

FIG. 7. Asymmetric flow patterns: absolute value of $w(z)$ for ascending flow (●) and descending flow (○) at various Rayleigh numbers: (a) $Ra = 2472$; (b) 3789; (c) 4878; (d) 6446; (e) 8300.

The values of the expansion coefficients w_1–w_5 were determined by a least-square fit to all numerical results. Thus we obtained $w_1 = 11.75$, $w_3 = 0.50$, $w_5 = 0.02$.

In our experimental work, the absolute values of maximum w-velocity in the ascending and descending flows ($w_{max(a)}$ and $w_{max(d)}$) have been measured very carefully at five different Ras covering the range $2472 < Ra < 8300$. These data were taken at $x > 2L_2$ to ensure fully developed flow. Each value was determined by first scanning in the y-direction at $z = 0.5H$ to find its local maximum and then by scanning in the z-direction to find its absolute maximum. Thus we accommodated possible asymmetries with respect to $z = 0.5H$. The results shown in Fig. 7 confirm the shift of the position of the maximum w-velocity at high Ra as predicted by the numerical solution. In addition, this figure shows a difference in the ascending and descending flows. This asymmetric roll pattern will be discussed in Section 4. The values of the various $w_{max(a)}$ and $w_{max(d)}$ are given in Table 2 together with average values w_{max} which were used for least-square fits of equation (9). Taking the temperature dependence of κ and ε (see Table 3) into account, we then obtained $w_1 = 12.72 \pm 0.12$, $w_3 = 0.12 \pm 0.10$, and $w_5 = 0.08 \pm 0.02$.

In Table 4 we compare the values of these expansion coefficients obtained from our numerical and experimental data with those from other theoretical [6, 8, 9] and experimental [10, 11] works. For the first harmonic (w_1), our results agree very well with others. Deviations for the higher harmonics can be understood in terms of the limited experimental accuracy and the averaging used for the suppression of the asymmetric behavior. Since the expansion in equation (9) is in terms of $\varepsilon^{n/2}$, which in the range investigated by us varies from $0.45 < \varepsilon < 3.86$, the least-square fit

Table 2. Measured w_{max} for different Rayleigh numbers

Ra	$w_{max(a)}$ (cm s^{-1})	$w_{max(d)}$ (cm s^{-1})	$\frac{w_{max(d)}}{w_{max(a)}}$	w_{max} (cm s^{-1})
2472	1.45	1.24	0.85	1.35
3789	2.60	2.40	0.92	2.50
4878	3.13	3.04	0.97	3.08
6446	4.01	3.95	0.98	3.98
8300	4.99	5.30	1.06	5.14

$w_{max(a)}$: absolute valve of maximum w-velocity for the ascending flow.

$w_{max(d)}$: absolute valve of maximum w-velocity for the descending flow.

w_{max}: average value $= (w_{max(a)} + w_{max(d)})/2$.

mine their values near the critical state where they are more easily obtained from the linearized governing equation [5]. In dimensionless form this equation can be written as

$$(D^2-a^2)(D^2-a^2-\sigma)(D^2-a^2-Pr\,\sigma)w = -Ra\,a^2 w \tag{10}$$

where D represents d/dz, and a and σ are the dimensionless wave number and 'time' constant (i.e. $w \propto f(z)\exp(iay+\sigma t)$), respectively. Degiorgio [9] determined the magnitude of w_1 near the critical situation by assuming $\sigma = 0$ in equation (10). The solution, w_1, which is Ra independent, obtained near the critical state should also be good for higher Ras.

Table 3. Operation conditions for N_0 at $P_0 = 0.85$ atm

T_c (K)	T_h (K)	T_0 (K)	ν (cm^2 s^{-1})	$g\beta/\nu^2$ (cm^{-3} K^{-1})	$Pr = \nu/\kappa$	Ra
296.0	305.4	300.7	0.186	93.9	0.71	2472
296.0	311.0	303.5	0.189	90.2	0.71	3789
296.0	316.0	306.0	0.192	87.1	0.71	4878
296.0	324.0	310.0	0.196	82.2	0.71	6446
296.0	335.0	315.5	0.202	76.0	0.71	8300

Note:
(1) P_0 is the pressure measured at the inlet of the isothermal section.
(2) Only the density has been corrected, through the ideal gas law, at $P_0 = 0.85$ atm.
(3) The physical properties are based on T_0 and calculated from ref. [25].

Table 4. Comparison with other works

	w_1	w_3	w_5	Pr
Analytical				
Busse (1967)†	12.08	0.3327	—	∞
Normand *et al.* [6]	11.82	0.1943	—	∞
Degiorgio [9]	10.64	—	—	—
Numerical				
This work	11.75	0.50	0.02	0.71
Experimental				
Dubois and Berge [10]	12.70 ± 0.04	0.35 ± 0.04	—	930
Dubois *et al.* [11]	12.28	—	—	11.1
This work	12.72 ± 0.12	0.12 ± 0.10	$0.08 + 0.02$	0.71

† Cited from Dubois and Berge [10].

needs to be carried to higher terms in $\varepsilon^{n/2}$ in order to get reliable coefficients. For example, if we had limited the above fit to the experimental data to the first two terms, $w_1 = 12.31 \pm 0.04$, and $w_3 = 0.50 \pm 0.02$ would have resulted.

In comparing the theoretical predictions and experimental results for different fluids (Pr), there are two interesting questions to ask. First, why can the theoretical prediction near the critical state, i.e. based on the expansion of the small parameter ε [6, 9], predict the correct flow structure up to such a high Ra (8300)? Secondly, why can the theoretical prediction based on an infinite Pr [6, 8] fit the data for such a wide range $0.71 < Pr < 930$? Actually, the answers to these two questions are tied together. First, since these expansion coefficients are independent of Ra, we can determine their values near the critical state where they are more easily obtained from the linearized governing equation [5]. In dimensionless form this equation can be written as

The answer to the second question lies in the term $Pr\,\sigma$ in equation (10). Since at the critical state, $\sigma = 0$, this term vanishes and the flow is Pr independent. Consequently, modes based on $Pr \to \infty$ can give good results (e.g. w_1-value) for slightly supercritical flows of any Pr.

4.4. *Asymmetric roll pattern*

The Boussinesq approximation with constant physical properties takes only the density variation in the z-direction into account and treats it as an external force in the z-momentum equation (4). Consequently, perfectly anti-symmetric (with respect to the center of the convection roll) flow behavior is obtained, as shown, for instance, in Figs. 6(a) and (b).

As depicted in Fig. 7, our experiments reveal an

asymmetric roll pattern even at the small temperature differences used between the horizontal plates (Table 3). At $2472 < Ra < 6446$, as listed in Table 2, $w_{max(a)} > w_{max(d)}$. The difference decreases with increasing Ra. At high Ra (8300), the trend is reversed.

Dubois *et al.* [11] also observed asymmetric rolls in water near 4°C with $w_{max(a)} > w_{max(d)}$. They attributed this asymmetry to the thermal expansion coefficient that varies from zero (top plate at 4°C) to finite values (bottom plate at a higher temperature). Hence, in their configuration the local driving forces are greater at the bottom plate than at the top.

For gases in the temperature range investigated, ν and κ vary with $T^{1.75}$, and Ra varies with $T^{-4.5}$ [21, 22]. Thus, according to equation (9), w_{max} should vary with $T^{-0.5}$. If one follows the local driving force argument, $w_{max(a)}$ (higher T, as shown in Fig. 6(c)) should be smaller than $w_{max(d)}$. But this is in contrast to our experimental findings at lower Ra (especially at $Ra = 2472$). Possible explanations of this effect may lie in the thermophoretic force acting on the seed particles [23, 24] in the direction from the hot plate to the cold plate. Hence, the thermophoretic force aids the seed particles in the ascending flow. In our experimental conditions the thermophoretic force has the same order of magnitude as the gravitational force [19]. At low Ras ($Ra = 2472$), where the asymmetry due to the temperature-dependent properties is expected to be small, the thermophoretic force is responsible for the difference ($w_{max(a)} > w_{max(d)}$). However, at high Ras ($Ra = 8300$), the asymmetry due to the temperature-dependent properties might overcome the thermophoretic force. This may lead to the reversal at high Ras.

5. SUMMARY

From a study of the velocity profiles of steady, fully developed, longitudinal rolls, in the range $2472 < Ra < 8300$ and $15 < Re < 150$, the following results were obtained.

(1) The governing equations for the transverse velocities (v and w) of the fully developed longitudinal convection rolls are shown analytically to be identical to those of 2-D R–B convection rolls. Thus, the critical Ra of the longitudinal convection rolls is equal to Ra_c; and the transverse velocities are independent of the forced-flow.

(2) The experimental results of w-velocity profiles confirm the above analytical results even far beyond the critical state (at Ra about $5Ra_c$).

(3) Numerical and experimental data for the expansion coefficients w_n (as used in equation (9)) for $Pr = 0.7$ (gases) are in good agreement with those found in other theoretical and experimental works for $Pr = 11.1$ and 930.

(4) The superposition of the forced flow, for $Ra_{c,t}(Re) > Ra > Ra_c$ where only longitudinal convection rolls exist, does remove the time dependence of R–B convection. Steady w-velocity profiles were measured up to $Ra = 8300$, as compared to the onset of time dependence of R–B flow in gases at $Ra > 4800$.

(5) The u-velocity is modulated by R–B convection rolls. The modulation amplitude as determined from the experimental profiles at $z = 0.5H$ is given by equation (7).

(6) Even at ΔTs of order 10°C, asymmetric flow patterns were observed as shown in Fig. 7. The asymmetry can be qualitatively understood in terms of the superposition of thermophoresis of the seed particles and the temperature-dependent properties of gases.

Acknowledgements—Support of this work by the Ceramics and Electronic Materials Program of the National Science Foundation under Grant DMR-8408398 is gratefully acknowledged. Clarifying discussions with Tom Nyce and Mike Banish are very much appreciated.

REFERENCES

1. R. Takahashi, Y. Koga and K. Sugawara, Gas flow pattern and mass transfer analysis in a horizontal flow reactor for chemical vapor deposition, *J. Electrochem. Soc.* **119,** 1406–1412 (1972).
2. B. J. Curtis, Convective effects in open-tube chemical vapor deposition, *PhysicoChem. Hydrodyn.* **2,** 357–366 (1981).
3. M. E. Braaten and S. V. Patankar, Analysis of laminar mixed convection in shrouded arrays of heated rectangular blocks, *Int. J. Heat Mass Transfer* **28,** 1699–1709 (1985).
4. K.-C. Chiu and F. Rosenberger, Mixed convection between horizontal plates—I. Entrance effects, *Int. J. Heat Mass Transfer* **30,** 1645–1654 (1987).
5. S. Chandrasekhar, *Hydrodynamic and Hydromagnetic Stability*. Dover, New York (1981).
6. C. Normand, Y. Pomeau and M. G. Velarde, Convective instability: a physicist's approach, *Rev. Mod. Phys.* **49,** 581–624 (1977).
7. P. Berge and M. Dubois, Rayleigh–Benard convection, *Contemp. Phys.* **25,** 535–582 (1984).
8. F. Busse, On the stability of two-dimensional convection in a layer heated from below, *J. Math. Phys.* **46,** 140–150 (1967).
9. V. Degiorgio, Single-mode dynamics of convective instabilities in a horizontal liquid layer, *Phys. Rev.* **A20,** 2193–2202 (1979).
10. M. Dubois and P. Berge, Experimental study of the velocity field in Rayleigh–Benard convection, *J. Fluid Mech.* **85,** 641–653 (1978).
11. M. Dubois, P. Berge and J. Wesfreid, Non Boussinesq convective structures in water near 4°C, *J. Phys.* **39,** 1253–1257 (1978).
12. Y. Mori and Y. Uchida, Forced convection heat transfer between horizontal flat plates, *Int. J. Heat Mass Transfer* **9,** 803–817 (1966).
13. Y. Ogura and A. Yagihashi, A numerical study of convection rolls in a flow between horizontal plates, *J. Met. Soc. Japan* **47,** 205–217 (1969).
14. G. J. Hwang and K. C. Cheng, A boundary vorticity method for finite amplitude convection in plane Poiseuille flow, *Proc. 12th Midwestern Mech. Conf.*, Vol. 6, pp. 207–220. Univ. of Notre Dame (1971).
15. K. Fukui, M. Nakajima and H. Ueda, The longitudinal vortex and its effects on the transport process in combined free and forced laminar convection between hori-

zontal and inclined parallel plates, *Int. J. Heat Mass Transfer* **26**, 109–120 (1983).
16. S. Ostrach and Y. Kamotani, Heat transfer augmentation in laminar fully developed channel flow by means of heating from below, *J. Heat Transfer* **97**, 220–225 (1975).
17. D. A. Nield, A note on the stability of laminar flow of a liquid mixture with temperature gradient, *Physica* **74**, 607–610 (1974).
18. M. S. Engelman, FIDAP, Fluid Dynamics Analysis Program, User/Theoretical Manual, Control Data Corporation, Pub. No. 84003650 (1983).
19. K.-C. Chiu, Mixed convection between horizontal plates and consequences for CVD flows, Ph.D. Dissertation, University of Utah, Salt Lake City, Utah (1986).
20. G. E. Willis and J. W. Deardorff, The oscillatory motions of Rayleigh convection, *J. Fluid Mech.* **44**, 661–672 (1970).
21. B. J. Curtis and J. P. Dismukes, Effects of natural and forced convection in vapor phase growth system, *J. Crystal Growth* **17**, 128–140 (1972).
22. L. J. Giling, Gas flow patterns in horizontal epitaxial reactor cells observed by interference holography, *J. Electrochem. Soc.* **129**, 634–644 (1982).
23. J. R. Brock, On the theory of thermal forces acting on aerosol particles, *J. Colloid Sci.* **17**, 768–780 (1962).
24. L. Talbot, R. K. Cheng, R. W. Schefer and D. R. Willis, Thermophoresis of particles in a heated boundary layer, *J. Fluid Mech.* **101**, 737–758 (1980).
25. W. M. Kays and M. E. Crawford, *Convective Heat and Mass Transfer*, 2nd Edn, p. 389. McGraw-Hill, New York (1980).

CONVECTION MIXTE EN PLAQUES HORIZONTALES—II. ECOULEMENT PLEINEMENT DEVELOPPE

Résumé—Les profils de vitesse pleinement développés des rouleaux de convection longitudinaux dans la convection mixte entre plaques horizontales sont mesurés dans l'azote par anémométrie laser Doppler pour un domaine $2472 < Ra < 8300$ et $15 < Re < 150$. On montre analytiquement et expérimentalement que les vitesses transversales des rouleaux de convection longitudinaux sont indépendants de l'écoulement forcé. Les profils de w expérimentaux et numériques ($Pr = 0{,}71$) sont en bon accord avec les prédictions théoriques ($Pr \to \infty$) et d'autres résultats expérimentaux ($Pr = 11{,}1$ et 930) pour la convection de Rayleigh–Benard. Une étude détaillée de la modulation de vitesse longitudinale $\Delta u[w_{max}(Re), Re]$ est présentée. Des configurations de rouleaux asymétriques sont aussi trouvées malgré des petites différences de température utilisées entre les plaques horizontales.

MISCH-KONVEKTION ZWISCHEN HORIZONTALEN PLATTEN—II. VOLL ENTWICKELTE STRÖMUNG

Zusammenfassung—Es wurden die voll entwickelten Geschwindigkeits-Profile von längsgerichteten Konvektionswalzen bei Mischkonvektion von Stickstoff zwischen horizontalen Platten mit einem Laser-Doppler-Anemometer in einem Bereich von $2472 < Ra < 8300$ und $15 < Re < 150$ gemessen. Es wird analytisch und experimentell nachgewiesen, daß die Querströmungsgeschwindigkeiten an der längsgerichteten Konvektionswalze unabhängig von der erzwungenen Strömung sind. Die experimentell und numerisch ermittelten w-Profile ($Pr = 0{,}71$) zeigen eine gute Übereinstimmung mit den theoretischen Voraussagen ($Pr \to \infty$) und anderen experimentellen Ergebnissen ($Pr = 11{,}1$ und 930) bei Rayleigh–Benard-Konvektion. Eine detaillierte Darstellung der Geschwindigkeitsschwanungen in Längsrichtung $\Delta u[w_{max}(Ra), Re]$ wird gezeigt. Trotz der geringen Temperaturdifferenz zwischen den beiden horizontalen Platten traten auch asymmetrische Walzenmuster auf.

СМЕШАННАЯ КОНВЕКЦИЯ МЕЖДУ ГОРИЗОНТАЛЬНЫМИ ПЛАСТИНАМИ—II. ПОЛНОСТЬЮ РАЗВИТОЕ ТЕЧЕНИЕ

Аннотация—Полностью развитые профили скорости продольных конвективных валов при смешанной конвекции между горизонтальными пластинами измерялись в азоте с помощью метода лазерной допплеровской анемометрии в диапазоне $2472 < Ra < 8300$ и $15 < Re < 150$. Аналитически и экспериментально показано, что поперечные скорости продольных конвективных валов не зависят от вынужденного течения. Полученные экспериментально и численно w-профили ($Pr = 0{,}71$) хорошо согласуются с результатами теоретических расчетов ($Pr \to \infty$) и другими экспериментальными данными ($Pr = 11{,}1$ и 930) для случая конвекции Рэлея–Бенара. Представлены результаты детального исследования колебаний продольной скорости $\Delta u[w_{max}(Ra), Re]$. Кроме того, наблюдались случаи осесимметричных валов несмотря на небольшой перепад температур между горизонтальными пластинами.